Available online at www.sciencedirect.com
ScienceDirect
Journal of Solid State Chemistry 181 (2008) 1048–1055
JOURNAL OF SOLID STATE CHEMISTRY
www.elsevier.com/locate/jssc

Cooperative self-construction and enhanced optical absorption of nanoplates-assembled hierarchical Bi_2WO_6 flowers

Shengwei Liu, Jiaguo Yu*

State Key Laboratory of Advanced Technology for Material Synthesis and Processing, Wuhan University of Technology, Luoshi Road 122#, Wuhan 430070, PR China

Received 26 October 2007; received in revised form 15 January 2008; accepted 20 January 2008
Available online 10 March 2008

Abstract

Bi_2WO_6 hierarchical multilayered flower-like assemblies are fabricated on a large scale by a simple hydrothermal method in the presence of polymeric poly(sodium 4-styrenesulfonate). Such 3D Bi_2WO_6 assemblies are constructed from orderly arranged 2D layers, which are further composed of a large number of interconnected nanoplates with a mean side length of ca. 50 nm. The bimodal mesopores associated with such hierarchical assembly exhibit peak mesopore size of ca. 4 nm for the voids within a layer, and peak mesopore size of ca. 40 nm corresponding to the interspaces between stacked layers, respectively. The formation process is discussed on the basis of the results of time-dependent experiments, which support a novel 'coupled cooperative assembly and localized ripening' formation mechanism. More interestingly, we have noticed that the collective effect related to such hierarchical assembly induces a significantly enhanced optical absorbance in the UV–visible region. This work may shed some light on the design of complex architectures and exploitation of their potential applications.

Keywords: Bi_2WO_6; Hierarchical assemblies; Flower-like; Cooperative assembly; Ripening; Enhanced optical absorbance

1. Introduction

A variety of biological minerals with fascinating shapes and microstructures was created in nature. Such natural materials are usually composed of only ordinary composition but exhibit fascinating properties due to their unique structure [1]. With expectation of achieving novel or enhanced properties, great efforts have been focused on the controlled synthesis of inorganic or inorganic/organic hybrid materials with specific shape or highly ordered construction [2–4]. Especially, the hierarchical assembly of 1D or 2D nanoscale building blocks into 3D arrayed superstructures or complex architectures attracts intensive attention, which would offer opportunities to explore their novel collective optical, magnetic, and electronic properties [5,6].

Bi_2WO_6 is one promising visible-light responsive photocatalyst [7–12]. The morphology and texture microstructures are usually important factors in modifying the photophysical and photocatalytic properties. Many preparative routes (such as solid-state, hydrothermal, sonochemical, etc.) and preparative conditions have been studied for the synthesis of Bi_2WO_6 with tunable morphology, such as nanoparticles, nanoplates, etc. [9–11]. In particular, hierarchical microspheres have been synthesized with or without polymer [13–16]. However, their formation mechanism is quite divergent.

Herein, we show that novel Bi_2WO_6 hierarchical multilayered flower-like assemblies can be easily fabricated by a hydrothermal process in the presence of poly(sodium4-styrenesulfonate), and a novel 'coupled cooperative assembly and localized ripening' formation mechanism is proposed. In addition, a significant enhancement of the optical absorbance in the UV–visible region associated with such hierarchical assembly has been observed, which

*Corresponding author. Fax: +86 27 87 879468.
E-mail address: jiaguoyu@yahoo.com (J. Yu).

0022-4596/$ - see front matter © 2008 Elsevier Inc. All rights reserved.
doi:10.1016/j.jssc.2008.01.049

may provide another new approach for increasing their photoactivity.

2. Experimental sections

2.1. Synthesis

All chemicals are of analytical grade, and used as received without further purification. Ordered assemblies of Bi_2WO_6 nanoplates were prepared by a simple polymer-mediated hydrothermal process. In a typical synthesis, 0.002 mol $Bi(NO_3)_3 \cdot 5H_2O$ and 0.001 mol Na_2WO_4 were added into 80 mL 1 g/L aqueous solution of poly(sodium4-styrenesulfonate) (PSS) (Aldrich, M_w ca. 1 000 000) under vigorous stirring. After stirring for another 15 min, the slurry solution was transferred into a 100 mL autoclave with a Teflon liner, which was then maintained at 180 °C for 18 h. Then, the reactor was cooled to room-temperature naturally in air. The yellow precipitate was collected and washed with distilled water for more than three times. As control experiments, Bi_2WO_6 nanoplates were also synthesized without polymer by a similar procedure. Both samples were dried at 80 °C for 6 h for characterization.

2.2. Characterization

X-ray powder diffraction (XRD) patterns were obtained on a D/Max-RB X-ray diffractometer (Rigaku, Japan) using Cu$K\alpha$ radiation at a scan rate of 0.05° $2\theta\,s^{-1}$. Scanning electron microscopy (SEM) was performed with a Hitachi-4800S microscope (Hitachi, Japan). Transmission electron microscopy (TEM) analysis was conducted using a JEM-2100F microscope (JEOL, Japan). The porous structure and Brunauer–Emmett–Teller (BET) surface area of the samples were analyzed by nitrogen adsorption in a Micromeritics ASAP 2020 nitrogen adsorption apparatus (USA). All the samples were degassed at 180 °C prior to nitrogen adsorption measurements. The BET surface area was determined by a multipoint BET method using the adsorption data in the relative pressure (P/P_0) range 0.05–0.3. Desorption isotherm was used to determine the pore size distribution via the Barret–Joyner–Halender (BJH) method, assuming a cylindrical pore modal [17–20]. The UV–visible diffuse reflectance spectra were obtained on a UV-2550 UV–visible spectrophotometer (Shimadzu, Japan). $BaSO_4$ was used as a reflectance standard in the UV–visible diffuse reflectance experiment.

3. Results and discussion

3.1. Hierarchical assemblies of Bi_2WO_6 nanoplates

Fig. 1 shows XRD patterns of as-prepared products obtained with and without PSS. The results demonstrate that well-crystallized Bi_2WO_6 crystals can be easily prepared whether the organic additive is added or not.

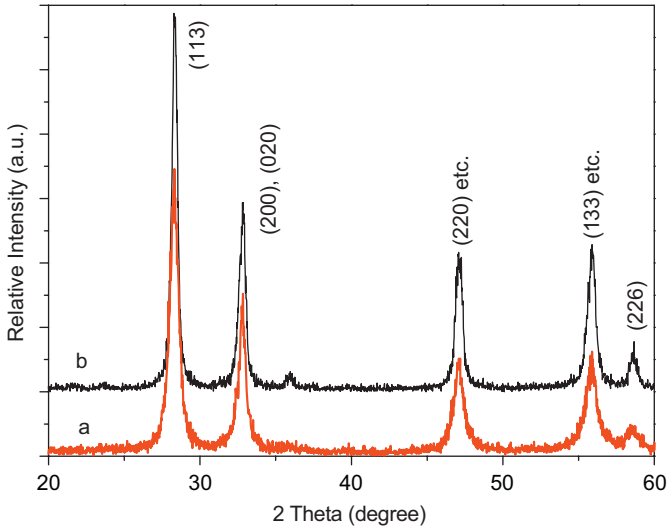

Fig. 1. XRD patterns of Bi_2WO_6 samples obtained in the presence (a) and absence (b) of PSS.

All the diffraction peaks can be readily indexed as a pure orthorhombic structure with cell parameters $a = 5.46$ Å, $b = 5.44$ Å and $c = 16.44$ Å, which is in good agreement with the literature values (JCPDS No. 73-1126) [11,13]. The presence of polymer in the synthetic system slightly inhibit the crystallization and the crystal growth of Bi_2WO_6, as evidenced by the increase of half-height width and decrease of relative intensity at the (113) peak corresponding to $2\theta = 28°$. On the other hand, it is interesting to note that the relative intensity of the (200) or (020) peak vs. (113) peak increases significantly as compared with that from the literature value, suggesting the special anisotropic growth of the crystals along (001) plane [11].

Fig. 2a is a typical SEM image of the products obtained with 1 g/L PSS after hydrothermal treatment at 180 °C for 18 h. Clearly, the 3D Bi_2WO_6 hierarchical assemblies with a flower-like configuration are constructed from many arranged 2D layers, and their average particle size is in the range of 2–3 μm. Except for some peeled square nanoplates, no other morphologies are observed. Higher magnification SEM image of the 2D layers (Fig. 2b and c) shows that they are further composed of densely packed nanoplates with an average side length of ca. 50 nm and a thickness of less than 20 nm. Even though, these complex superstructures are sufficiently stable they could not be broken into discrete nanoplates even after 10 min ultrasonication. The features of such complex assemblies are further investigated by TEM results (Fig. 3). An individual Bi_2WO_6 flower presented in Fig. 3a confirms its particle diameters of 2–3 μm. The light–dark contrast reflects an asymmetric distribution of the building blocks, which conforms to the multilayered flower-like structures (Fig. 2a). An enlarged TEM image (Fig. 3b) of the outer edges shows that the local primary nanobuilding blocks are mainly irregular nanoplates, instead of square nanoplates.

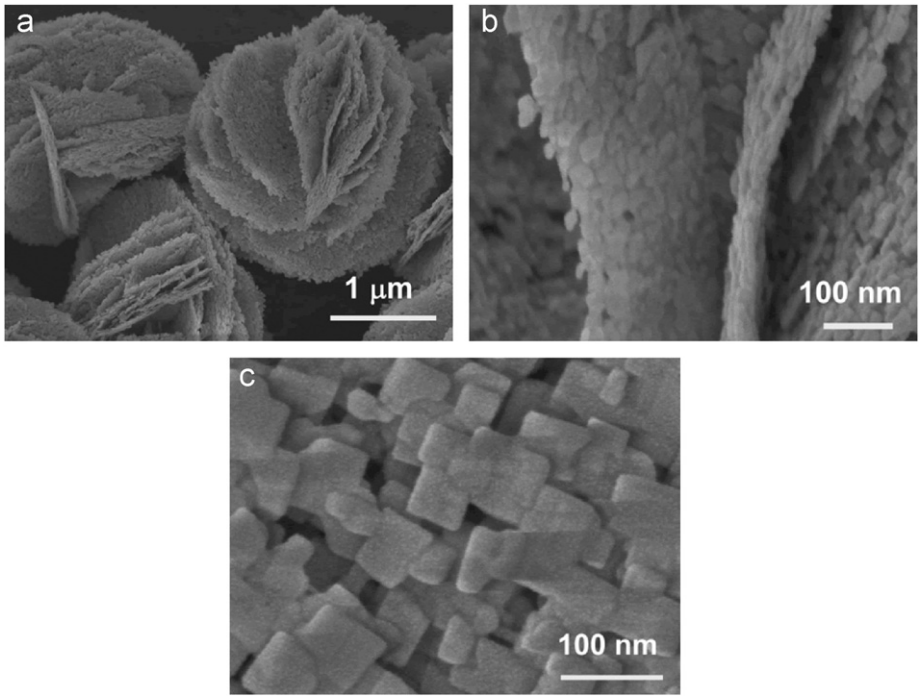

Fig. 2. SEM images of Bi_2WO_6 flowers obtained with PSS: (a) overall morphology; (b) side view and (c) top view of individual 2D layer.

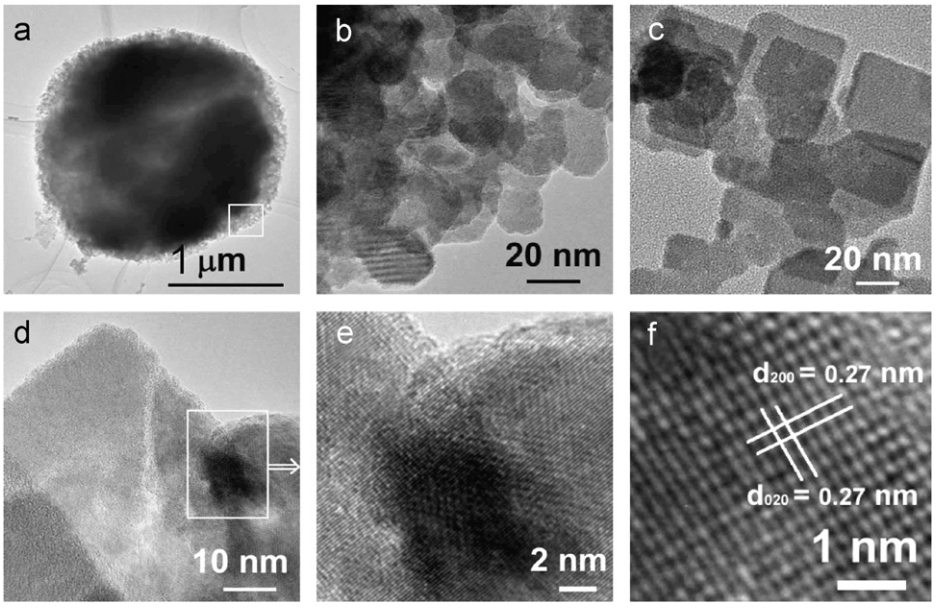

Fig. 3. TEM images of Bi_2WO_6 flowers obtained with PSS: (a) overall morphology of an individual flower; (b) detailed view of the outer edge of a 2D layer circled in a; (c) higher magnification TEM image of the peeled fragments; (d, e) higher magnification TEM image of two adjacent nanoplates fused by oriented attachment; (f) high-resolution TEM image of the nanoplate.

Moreover, their grain sizes are generally in the range of 20–30 nm, which is smaller than that reflected by SEM image (Fig. 2b and c). These results imply that, those nanoplates toward the outer edge are underdeveloped intermediates, during the progressive evolution of the 2D layers. Such an opinion has been readily confirmed. The fragments scaled off during the ultrasonic dispersion are indeed larger well-developed square nanoplates (Fig. 3c), which is similar to that reflected by SEM in Fig. 2c. Therefore, a ripening process regulated by both the thermodynamic aspects and the inherent crystal structure of Bi_2WO_6 is expected for the evolution of those primary nanobuilding blocks. In addition, an interesting oriented attachment process [3,4,21,22] is also observed. As shown in Fig. 3d and e, two adjacent nanoplates are fused together as one side-to-side, forming a crystallographically

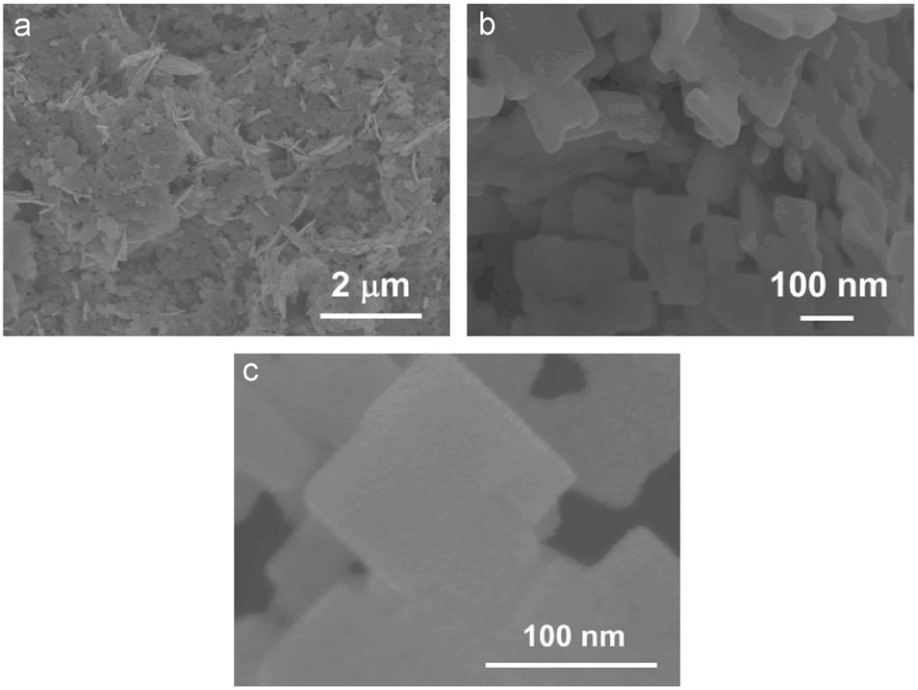

Fig. 4. SEM images of Bi_2WO_6 leaves obtained in pure water: (a) overall morphology; (b, c) higher magnification.

continuous interface. A typical high-resolution TEM image (Fig. 3f) demonstrates the single-crystal feature of an individual nanobuilding block. The spacing of the lattice fringes are measured to be with an almost identical value of ca. 0.27 nm, corresponding to the (200) and (020) planes of Bi_2WO_6 [14]. This result confirms its special anisotropic growth along (001) plane, as initially reflected by the XRD results.

The presence of PSS in the present synthetic system may be critical for the formation of those Bi_2WO_6 flowers. As compared, the product obtained without PSS under identical conditions exhibits leaf-shaped morphology (Fig. 4a), which is somewhat similar to the previous results [11,23,24]. Higher magnification SEM images (Fig. 4b and c) show those leaves are the 2D assemblies of square nanoplates with average side length of ca. 60 nm.

The hierarchical self-assembly related to those Bi_2WO_6 flowers endows them with hierarchically porous structures. Fig. 5 shows the nitrogen sorption isotherms. The isotherm corresponding to Bi_2WO_6 leaves is of type IV (BDDT classification) with a hysteresis loop at high relative pressures, indicating their mesoporous feature [17]. The shape of the hysteresis loop is of type H3, suggesting narrow slit-shaped pores that are generally associated with plate-like particles [17], which agrees well with their morphology (Fig. 4). Interesting, the hysteresis loop corresponding to Bi_2WO_6 flowers is significantly left-shifted up to 0.4 (as compared with that of Bi_2WO_6 leaves within 0.8–1), implying the bimodal mesopore size distribution, which was confirmed by the corresponding pore size distribution in the inset in Fig. 5. The Bi_2WO_6

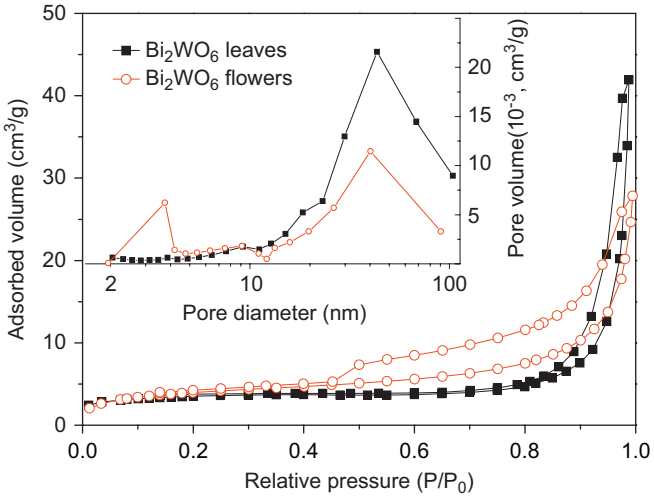

Fig. 5. Nitrogen sorption isotherms and the corresponding pore size distribution curves (inset) of the Bi_2WO_6 flowers and leaves.

flowers contain small mesopores (ca. 4 nm) and larger mesopores with a maximum pore diameter of ca. 40 nm. Combined with the above SEM and TEM results, the smaller mesopores are related to the voids formed between plate-like primary nanobuilding blocks within a layer, and the larger mesopores are associated with interspaces produced between stacked 2D layers. Besides, both samples exhibit macropores with pore sizes up to 100 nm. In addition, as expected, the specific surface area of Bi_2WO_6 flowers is slightly larger than that of Bi_2WO_6 leaves.

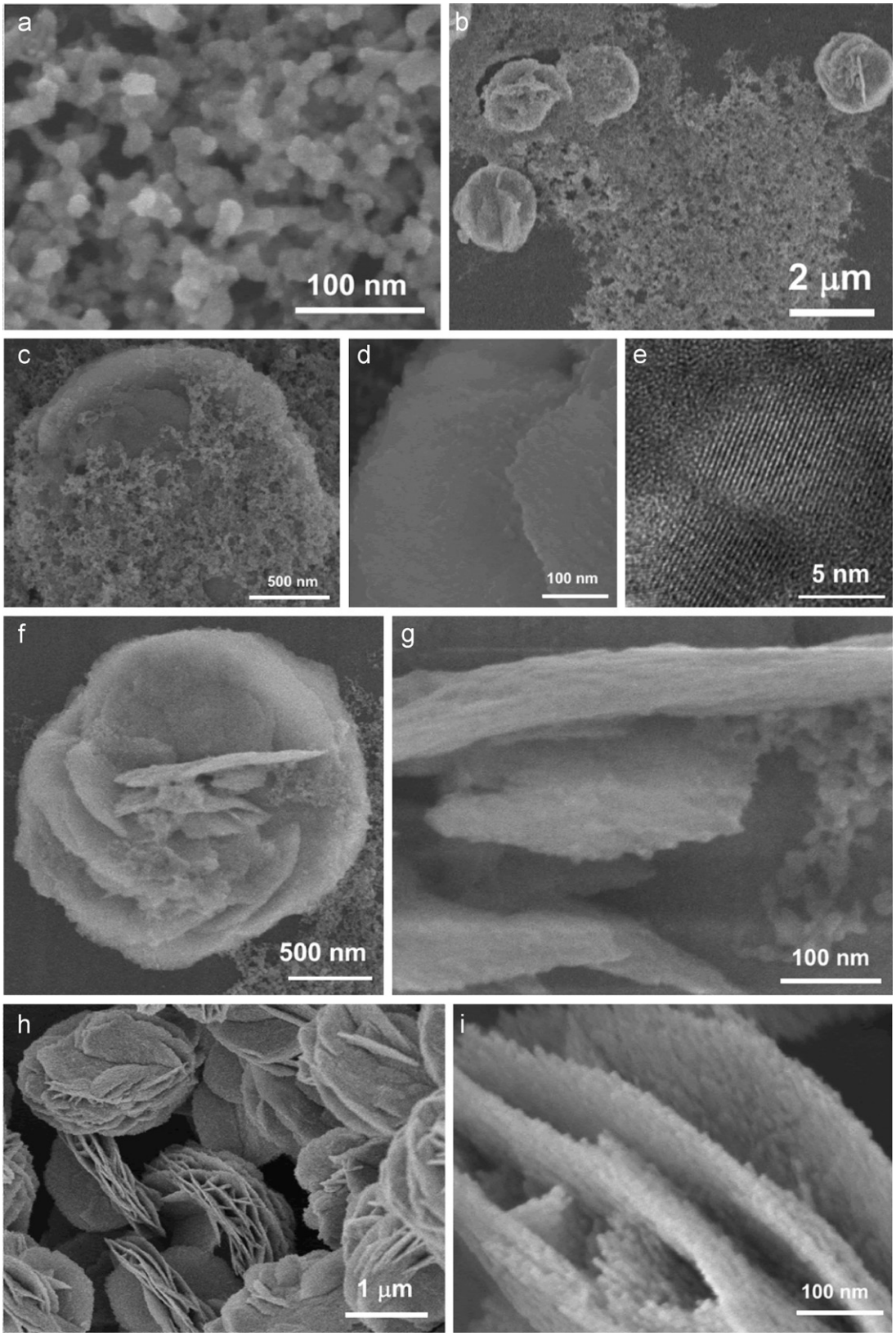

Fig. 6. SEM and TEM images of Bi_2WO_6 samples obtained in the presence of PSS with various reaction times: (a) 0.5 h; (b–g) 2 h; (h, i) 8 h.

3.2. Formation process

The formation of hierarchical architecture has been a focus of recent studies in terms of the nonclassical crystallization process [4]. The similar hierarchical assemblies, constructed from nanoplates, have also been previously observed for the synthesis of ZnO, YBO_3, etc. [25,26]. However, the formation mechanism accounting for

such hierarchical assemblies is still quite divergent, and further detailed investigations are always required.

The time-dependent evolution experiments are carefully conducted to reveal the formation process of those Bi_2WO_6 flowers. The products were collected at different stages from the reaction mixture, and then their morphologies were investigated by SEM and TEM measurement. As shown in Fig. 6a, numerous nanoparticles with average size of ca. 20 nm are attained initially (30 min), which are proved to be amorphous by XRD results (Fig. 7a). After 2 h of reaction, some self-assembled multilayered structures (Fig. 6b) with average size of ca. 2 μm are detected in addition to those tiny nanoparticles. Higher magnification SEM images of the self-assembled layers (Fig. 6c and d) show that the layer is derived from the assembly of nanoparticles. Moreover, such assembly of amorphous nanoparticles is coupled with their dissolution and recrystallization processes, which is proved by the corresponding XRD pattern (Fig. 7b) and TEM image (Fig. 6e). The average crystalline size is estimated to be 10 nm from the broadening of (113) diffraction peak using Scherrer equation, which is confirmed by the TEM result. In addition, higher magnification SEM images of an underdeveloped multilayered flower are presented in Fig. 6f and g. Interesting, between two preformed layers, a newborn layer of self-assembled nanoparticles is developing, which may be the reason for the detachment and the curvature of initial closely stacked flat layers. After an additional 6 h of reaction, the products are exclusively layered assemblies (Fig. 6(h), while the initial amorphous nanoparticles are depleted. Besides, the nanocrystals within the layer obviously grow in size (Fig. 6i), which is confirmed by the XRD result (Fig. 7c). With further prolonging reaction duration, the layered assemblies are well-developed into the final flower-like configuration (Fig. 2a). During this process, both the layers themselves and their mutual coassembly further develop, along with the nanoparticles within the layer evolving as nanoplates.

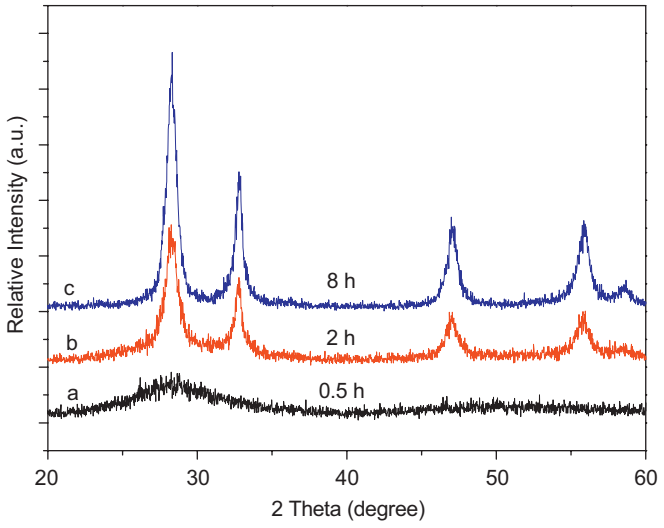

Fig. 7. XRD patterns of Bi_2WO_6 samples obtained in the presence of PSS with various reaction times: (a) 0.5 h; (b) 2 h and (c) 8 h.

According to the above results, the formation mechanism of those Bi_2WO_6 flowers is proposed as 'coupled cooperative assembly and localized ripening'. In short, the primary self-assembly of polymer-stabilized nanoparticles into 2D layers and the collective coassembly of as-forming layers into 3D superstructures occur simultaneously, accompanying with intricate crystal evolution processes within individual layer. Such a formation process is quite different from previously suggested, in which assembly usually proceed with stable preformed crystalline building blocks [13,15,27].

The main steps are schematically illustrated in Fig. 8. Initially, a large number of PSS-stabilized amorphous nanoparticles are formed in the supersaturated reaction

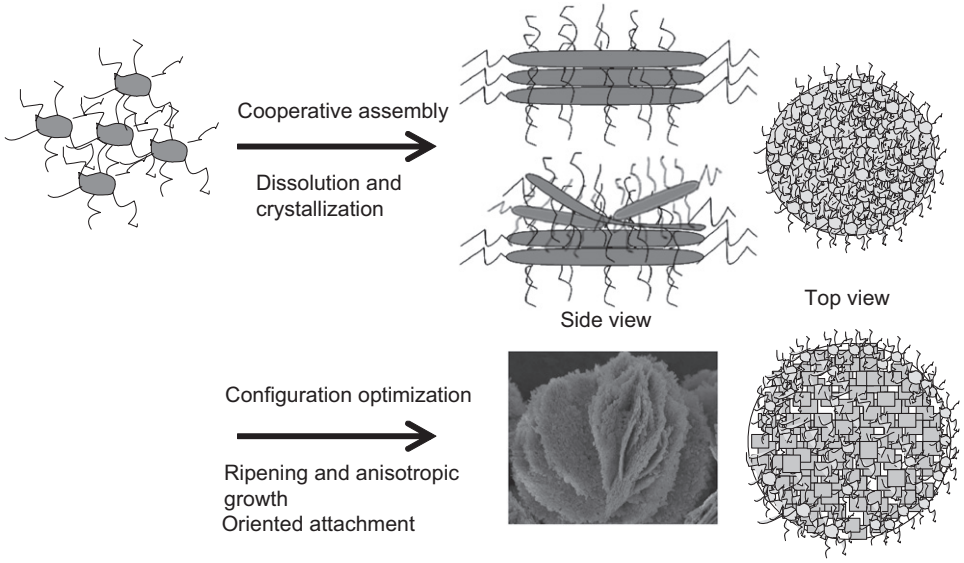

Fig. 8. Schematic illustration of the formation processes for as-prepared Bi_2WO_6 hierarchical multilayered flower-like assemblies.

systems. Subsequently, the polymeric PSS in solution will induce their aggregation by enthalpic changes (surface binding and interparticle bridging), as well as nonadsorption entropic mechanisms (depletion flocculation) [3]. Significantly, the onset of aggregation is coupled temporally with crystallization in the present case. Directed by the special intrinsic crystal structure of Bi_2WO_6 [11], together with the interfacial effect of ionic PSS molecules, anisotropic plate-like primary nanocrystals are favored. As a result, steric, van der Waals and hydrophilic–hydrophobic interactions associated with the pendent chains of the adsorbed PSS polymers, cooperative with the oriented attachment and dipole–dipole interactions associated with the special shape anisotropy of primary Bi_2WO_6 nanoplates [28,29], drive the spontaneous assembly of those polymer-anchored primary Bi_2WO_6 nanoparticles preferentially into secondary organic–inorganic composite 2D layers, which are further stacked in a layer-by-layer style due to the strong hydrophobic interactions between surface-absorbed polymers [3]. Occasionally, a new layer of self-assembled nanoparticles is developed between two preformed layers, which may function as a wedge resulting in the curvature of the top layer. In addition, the internal strain associated with such curvature facilitates the secondary nucleation occurring preferentially at such defect sites, giving rise to additional layers. Finally, a progressive self-modification process occurs in the synthetic solution, resulting in the final well-ordered flower-like configuration. Such an interesting organic–inorganic cooperative self-assembly modal involved here may be a general strategy and could be readily extended to other systems for complex hierarchical architectures.

During such assembly processes, a complex crystal evolution process of primary building blocks, involving Ostwald ripening, anisotropic growth, and oriented attachment, proceeds simultaneously within individual layer. After initial dissolution and renucleation, the larger crystallites grow at the cost of the smaller ones due to higher solubility of relatively smaller particles according to the Gibbs–Thomson law [13,30–32]. In a further crystallization process, the high anisotropy characteristics of Bi_2WO_6 [11], in combination with the selective adsorption effect of PSS, the layered localized evolution environments, result in the formation of square nanoplates. Meanwhile, the oriented attachment process of adjacent plate-like nanocrystals occurs in a side-to-side feature. Such a complex evolution process of primary building blocks, accompanying with the assembly process, has seldomly been reported previously.

3.3. Enhanced optical absorption

Fig. 9 presents the UV–visible diffuse reflectance spectrum of those hierarchical Bi_2WO_6 flowers, as compared with that of Bi_2WO_6 leaves obtained without any polymer. Both samples showed a great increase in absorption with wavelengths lower than ca. 450 nm, which

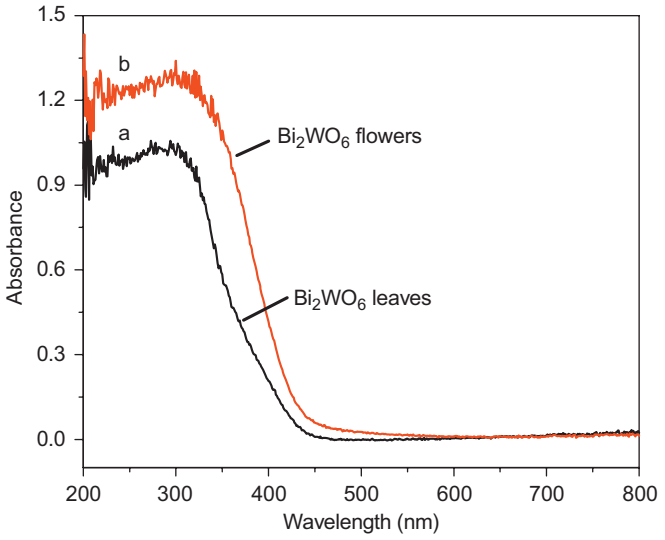

Fig. 9. UV–visible diffuse reflectance spectra of the Bi_2WO_6 flowers and leaves.

is associated with the intrinsic band gap absorption of Bi_2WO_6. In comparison with that for Bi_2WO_6 leaves, a notable red-shift in the absorption edge is observed for those hierarchical Bi_2WO_6 flowers, implying a smaller band gap. The variation in the electronic structures may be related to the collective effect associated with such hierarchical assembly, taking account of their similar shape and comparable crystallite size of primary building blocks. More interesting, a significantly enhanced optical absorbance in the UV–visible region is achieved for those Bi_2WO_6 hierarchical multilayered flower-like assemblies, about 30% higher than that for the Bi_2WO_6 leaves. The specific hierarchical configuration, along with their bimodal mesoporous microstructure, of those multilayered flower-like assemblies allows multiple scattering of UV–visible light within their frameworks, endowing them with even greater light-harvesting capacities [18–20]. In other words, the optical path length for light transporting through those Bi_2WO_6 hierarchical multilayered flower-like assemblies may be longer than that for nanoplates due to multiple scattering, resulting in a greater absorbance based on the famous Beer–Lambert Law [33]. It is expected that such a novel model, enhancing optical absorption by hierarchical assembly, provide another effective approach for increasing the photo-reactivity of semiconductors, and for other applications related to absorbing photons. Further work will aim at extending such a model towards other systems and exploiting their related applications.

4. Conclusions

Bi_2WO_6 hierarchical multilayered flower-like assemblies, constructed from primary nanoplates, are fabricated on a large scale by a simple polymeric PSS-mediated hydrothermal method. Such Bi_2WO_6 flowers exhibit bimodal mesopores due to hierarchical assembly. The peak

mesopore size for the voids within a layer is ca. 4 nm, while the peak mesopore size corresponding to the interspaces between stacked layers is ca. 40 nm. The formation mechanism is proposed as 'coupled cooperative assembly and localized ripening'. The self-assembly of polymer-stabilized nanoparticles into 2D layers proceeds simultaneously with the 3D mutual coassembly of as-forming layers, due to the organic–inorganic interfacial cooperative interactions. Meanwhile, intricate crystal evolution processes within individual layer occur, including dissolution and renucleation of amorphous nanoparticles, Ostwald ripening and anisotropic growth of primary nanocrystals as well as their oriented attachment. More interestingly, a significantly enhanced optical absorbance in the UV–visible region is observed, which is ascribed to the lengthened optical path length for light transporting as a result of multiple scattering within the hierarchical assemblies.

Acknowledgments

This work was partially supported by the National Natural Science Foundation of China (20473059, 50625208 and 20773097). This work was also financially supported by the Key Research Project of Chinese Ministry of Education (No. 106114) and National Basic Research Program of China (2007CB613302).

References

[1] S. Mann, G.A. Ozin, Nature 382 (1996) 313.
[2] Y. Yin, A.P. Alivisatos, Nature 437 (2005) 664.
[3] H. Colfen, S. Mann, Angew. Chem. Int. Ed. 42 (2003) 2350.
[4] H. Colfen, M. Antonietti, Angew. Chem. Int. Ed. 44 (2005) 5576.
[5] M. Li, H. Schnablegger, S. Mann, Nature 402 (1999) 393.
[6] M.P. Pileni, J. Phys. Chem. B 105 (2001) 3358.
[7] A. Kudo, S. Hijii, Chem. Lett. 10 (1999) 1103.
[8] J.W. Tang, Z.G. Zou, J.H. Ye, Catal. Lett. 92 (2004) 53.
[9] J.G. Yu, J.F. Xiong, B. Cheng, Y. Yu, J.B. Wang, J. Solid State Chem. 178 (2005) 1968.
[10] S. Zhang, C. Zhang, Y. Man, Y. Zhu, J. Solid State Chem. 179 (2006) 62.
[11] C. Zhang, Y. Zhu, Chem. Mater. 17 (2005) 3537.
[12] H. Fu, C. Pan, W. Yao, Y. Zhu, J. Phys. Chem. B 109 (2005) 22432.
[13] Y.Y. Li, J.P. Liu, X.T. Huang, G.Y. Li, Cryst. Growth Des. 7 (2007) 1350.
[14] L. Zhang, W. Wang, Z. Chen, L. Zhou, H. Xu, W. Zhu, J. Mater. Chem. 17 (2007) 2526.
[15] L. Zhang, W. Wang, L. Zhou, H. Xu, Small 3 (2007) 1618.
[16] J. Wu, F. Duan, Y. Zheng, Y. Xie, J. Phys. Chem. C 111 (2007) 12866.
[17] K.S.W. Sing, D.H. Everett, R.A.W. Haul, L. Moscou, R.A. Pierotti, J. Rouquerol, T. Siemieniewska, Pure Appl. Chem. 57 (1985) 603.
[18] J.G. Yu, S.W. Liu, H.G. Yu, J. Catal. 249 (2007) 59.
[19] J.G. Yu, Y.R. Su, B. Cheng, Adv. Funct. Mater. 17 (2007) 1984.
[20] J.G. Yu, L.J. Zhang, B. Cheng, Y.R. Su, J. Phys. Chem. C 111 (2007) 10582.
[21] X.F. Wang, J.B. Xu, N. Ke, J.G. Yu, J. Wang, Q. Li, H.C. Ong, R. Zhang, Appl. Phys. Lett. 88 (2006) 223108.
[22] R.L. Penn, J.F. Banfield, Science 281 (1998) 969.
[23] L. Yang, P.W. May, L. Yin, T.B. Scott, Nanotechnology 18 (2007) 215602.
[24] L. Yang, P.W. May, L. Yin, T.B. Scott, J.A. Smith, K.N. Rosser, Nanotechnology 17 (2006) 5798.
[25] J.B. Liang, J.W. Liu, Q. Xie, S. Bai, W.C. Yu, Y.T. Qian, J. Phys. Chem. B 109 (2005) 9463.
[26] X.-C. Jiang, L.-D. Sun, C.-H. Yan, J. Phys. Chem. B 108 (2004) 3387.
[27] S.W. Liu, J.G. Yu, B. Cheng, L. Zhao, Q.J. Zhang, J. Cryst. Growth 279 (2005) 461.
[28] S. Zhang, X. Li, Colloid Surf. A 226 (2003) 35.
[29] S. Zhang, J. Shen, H. Fu, W. Dong, Z. Zheng, L. Shi, J. Solid State Chem. 180 (2007) 1456.
[30] J.G. Yu, H.T. Guo, S.A. Davis, S. Mann, Adv. Funct. Mater. 16 (2006) 2035.
[31] H.G. Yu, J.G. Yu, S.W. Liu, S. Mann, Chem. Mater. 19 (2007) 4327.
[32] J.G. Yu, H.G. Yu, H.T. Guo, M. Li, S. Mann, Small 4 (2008) 87.
[33] W.-Q. Han, L. Wu, R.F. Klie, Y. Zhu. Adv. Mater. 19 (2007) 2525.